Journal of Biomechanics 95 (2019) 109320

Contents lists available at ScienceDirect

Journal of Biomechanics

journal homepage: www.elsevier.com/locate/jbiomech
www.JBiomech.com

Mandibular biomechanics after marginal resection: Correspondences of simulated volumetric strain and skeletal resorption

Cornelia Kober [a,*], Göran Kjeller [b], Christian Hellmich [c], Robert Alexander Sader [d], Britt-Isabelle Berg [e,f]

[a] Hamburg University of Applied Sciences, Leuschnerstr. 25, D-21031 Hamburg, Germany
[b] Department of Oral & Maxillofacial Surgery, Institute of Odontology, The Sahlgrenska Academy, PO Box 450, SE-40530 Gothenburg, Sweden
[c] Institute for Mechanics of Materials and Structures, Vienna University of Technology, Karlsplatz 13/202, A-1040 Vienna, Austria
[d] Mund-, Kiefer- und Plastische Gesichtschirurgie, Klinikum und Fachbereich Medizin, Johann Wolfgang Goethe University Frankfurt am Main, Theodor-Stern-Kai 7, D-60596 Frankfurt am Main, Germany
[e] Klinik für Mund-, Kiefer- und Gesichtschirurgie, University Hospital Basel, Spitalstr. 21, CH-4031 Basel, Switzerland
[f] Hightech Research Center of Cranio-Maxillofacial Surgery (HFZ), University Hospital Basel, Gewerbestrasse 14, CH-4123 Allschwil, Switzerland

ARTICLE INFO

Article history:
Accepted 14 August 2019

Keywords:
Mandible
Marginal mandibulectomy
Finite element simulation
Skeletal adaptation
3D-visualization

ABSTRACT

Serious mandibular diseases such as tumor or osteonecrosis often require segmental or marginal mandibulectomy, the latter with improved outcome thanks to preserved mandibular continuity. Nevertheless, gradual osteolytic and/or osteosclerotic skeletal changes frequently indicate repetitive resections. Based on the fundamental adaptivity of bone to mechanical loads, the question arose whether resection-related anatomical alterations trigger relevant pathological skeletal adaptations. For a clinical case after mandibular box resection due to progressive osteoradionecrosis (ORN), routine biomechanical loading was simulated by finite element method, respecting pathology-related anatomy, tissue properties, and biting capacity. By 3D-visualization of the mandible's pathological development from follow-up-CT's over four years, remarkable correspondences of skeletal resorptions and increased unphysiological strain were revealed. Higher unphysiological load was correlated with more serious and earlier skeletal alterations. Three months post-operatively, serious buccal destruction at the distal resection corner occurred in correspondence with dominant tensile strain. At the resection, elevated strain caused by reduced alveolar height corresponded to skeletal compromise, observed 8–9 months post-operatively. ORN-related lesions, diagnosed before resection, entailed unphysiological strain coinciding with local skeletal alterations. Simulations with "healthy" instead of pathological tissue coefficients induced quantitative improvements of 25–33%, but without fundamental change. These results suggest a decisive contribution of resection-related biomechanical skeletal adaptations to this patient's mandibular decline with hemimandibulectomy about 2.5 years after the first resection. However, mechanical stress concentrations in sharp angles as the distal resection corner and reduced stability due to decreased alveolar height generally bear the danger of pathological biomechanics and severe skeletal adaptations for patients after mandibular box resection.

1. Introduction

Surgical resections of the mandible indicated, e.g., by osseous tumors or severe osteonecrosis often have serious consequences for patients' quality of life (Massa et al., 2017). Differently from segmental resection, by marginal mandibulectomy, only a portion of the mandible is removed with preserved mandibular continuity. Though improved outcome (Muñoz Guerra et al., 2003; Wax, 2005), also these interventions frequently show adverse effects as facial disfigurement, limited mouth opening, difficulties in swallowing solid food, and other essential activities of daily living (Massa et al., 2017; Vijayaraghavan et al., 2015). Often, due to progressive skeletal compromise, repetitive resections are necessary up to hemi- or complete mandibulectomy.

Regarding the fundamental adaptivity of bone to mechanical loads (Wolff, 1892), the question arose whether resection-related alterations of the patients' physiological load carrying behavior entail skeletal adaptations, proving pathological biomechanics as potential further burden for affected patients besides primary diseases. Preliminary finite element analysis (FEA) endorsed this assumption (Kober et al., 2016).

* Corresponding author.
E-mail address: c.kober.hamburg@gmail.com (C. Kober).

https://doi.org/10.1016/j.jbiomech.2019.109320
0021-9290/

Nomenclature

Abbreviations and symbols

3D	three-dimensional
CT	computed tomography
E	Young's modulus
FE	finite element
FEA	finite element analysis
FoV	field of view
HU	Hounsfield
ICP	clenching in intercuspal position
INC	incisal biting
LGF	lateral group effort
ν	Poisson's ratio
ORN	osteoradionecrosis
PDL	periodontal ligament
RMOL	contralateral first molar biting
TMJ	temporomandibular joint

Finite Element models

M1-inhomog	FE-model with inhomogeneous pathological elastic coefficients
M2-strong	FE-model with homogeneous "healthy" elastic coefficients for cortical respectively trabecular bone
M3-mean	FE-model with homogeneous elastic coefficients averaged over cortical respectively trabecular elastic coefficients of M1-inhomog

Skeletal adaptation due to mechanical loading was hypothesized in 1892 by "Wolff's law" (Wolff, 1892). Though still missing explicit mathematical formulation, there is a general agreement about an essential role of strain (e.g., Frost, 1994). The relation between mandibular biomechanics and its outer shape and inner architecture has been elaborately investigated. Anthropologists affirmed the biomechanical background of mandibular morphology (e.g., Daegling and Hylander, 2000; Williams et al., 2009). Orofacial adaptation was reported in dental implantology (e.g., Chou et al., 2008), prosthodontics (e.g., Li et al., 2016), or orthodontics (e.g., Wang et al., 2014). Researchers observed correspondences of the spatial distribution of Hounsfield (HU) values from computed tomography (CT) and regionally increased stress/strain during routine biting. Referring to the correlation of HU-values and tissue density (Kalender, 2011), they deduced the coherence of mandibular biomechanics and skeletal tissue density (e.g., Chou et al., 2015; Gröning et al., 2012; Kober et al., 2003; Kober et al., 2017; Pérez et al., 2010; Reina et al., 2007). Though evaluating different indicator variables, exemplarily maximal and minimal principal strain (e.g., Williams et al., 2009), strain energy density (e.g., Suenaga et al., 2015), von Mises equivalent strain (e.g., Gröning et al., 2012), volumetric strain (e.g., Hellmich et al., 2008), Frost's mechanostat theory (e.g., Mahnama et al., 2013), or remodelling algorithms (e.g., Pérez et al., 2010), all cited studies supported the hypothesis of mandibular skeletal adaptation due to mechanical load at clinically relevant dimensions.

FE-based research about marginal mandibulectomy has been focused on the mechanical stability of the jaw for prevention of pathological fracture (Murakami et al., 2011; Ertem et al., 2013). Both research groups reported excessive stress in the distal resection angle. Using FE-models constructed by CAD-software, (Murakami et al., 2011) identified sharp resection angles, reduced alveolar height, and occlusal forces as critical factors. (Ertem et al., 2013) created FE-models from a cadaver mandible without resection where they afterwards induced excisions by CAD-Software. Clinical cases have not been analyzed so far.

This article is dedicated to mandibular biomechanics and skeletal adaptation after marginal mandibulectomy. For a clinical case after mandibular box resection due to progressive osteoradionecrosis (ORN), routine biomechanical loading with reduced biting capacity is simulated applying ORN-related as well as "healthy" tissue coefficients. The pathological development of the skeletal structure over four years, visualized from follow-up-CT's, is compared with post-operative volumetric strain. The FEA has been performed using Kaskade (ZIB Berlin, Berlin, Germany; Erdmann et al., 1993). For image processing, segmentation, and visualization, Amira® 4.x-6.x (ZIB Berlin and Thermo Fisher Scientific, Berlin, Germany; Stalling et al., 2005) has been used.

2. Methods

2.1. Patient and radiology

Mandibular box resection was performed for a patient (male, 47 years) due to severe ORN after high dose radiotherapy concerning a left-sided T4 tonsil carcinoma (Fig. 1, top left). Generally, ORN shows signs of osteolytic and osteosclerotic processes (Obinata et al., 2017). In CT, osteolysis is imaged by reduced HU-units and osteosclerosis by increased HU-units. About two years later, further marginal mandibulectomy was indicated (Fig. 1, bottom left) with, three months later, hemimandibulectomy. Before hemimandibulectomy, six follow-up-CT's were acquainted by the same machine with similar protocols (Table 1). The FEA refers to follow-up-CT 3. Only follow-up-CT 6 covers the complete mandible.

2.2. Skeletal tissue visualization

Owing to its largest FoV, all follow-up-CT's were registered to follow-up-CT 6 and up-sampled to identical dimensions (0.2617 mm pixel side, 0.4 mm vertical slice distance) for simultaneous processing of all registered data. Following (Kober and Kjeller, 2015), mandibular bone was segmented from all (processed) follow-up-CT's. These segmentations were superimposed. The combined segmentation was grown in the axial CT-slices by about 2 mm delivering an envelope covering the mandible at all time steps plus a small soft tissue rim. The voxels outside the envelope were set to below the minimal HU-value, e.g., −10000, in all processed follow-up-CT's. Given the correlation of HU-values and (optical) tissue density (Kalender, 2011), transparent volume rendering with appropriate transfer function and physical color scale delivered a free view to 3D-profiles representing mandibular skeletal density (Fig. 5a–c and e–g). By the rim around the bone, the interface bone – surrounding tissue including ORN-related disarrangement was also visualized.

2.3. Generation of the FE-model

As the follow-up-CT 3 after the first resection covers only the mandibular corpus, contralateral (right) ramus and condyle were supplemented from follow-up-CT 6 (possible by registration and subsequent upsampling). Due to too high ipsilateral skeletal destruction in follow-up-CT 6, the voxels of the contralateral ramus and condyle were mirrored and registered re-establishing complete mandibular image data (Fig. 1). Moderate differences between the single data sets were equalized by 3D-Gaussian smoothing. Thereafter, cortical and trabecular bone, teeth, and temporomandibular

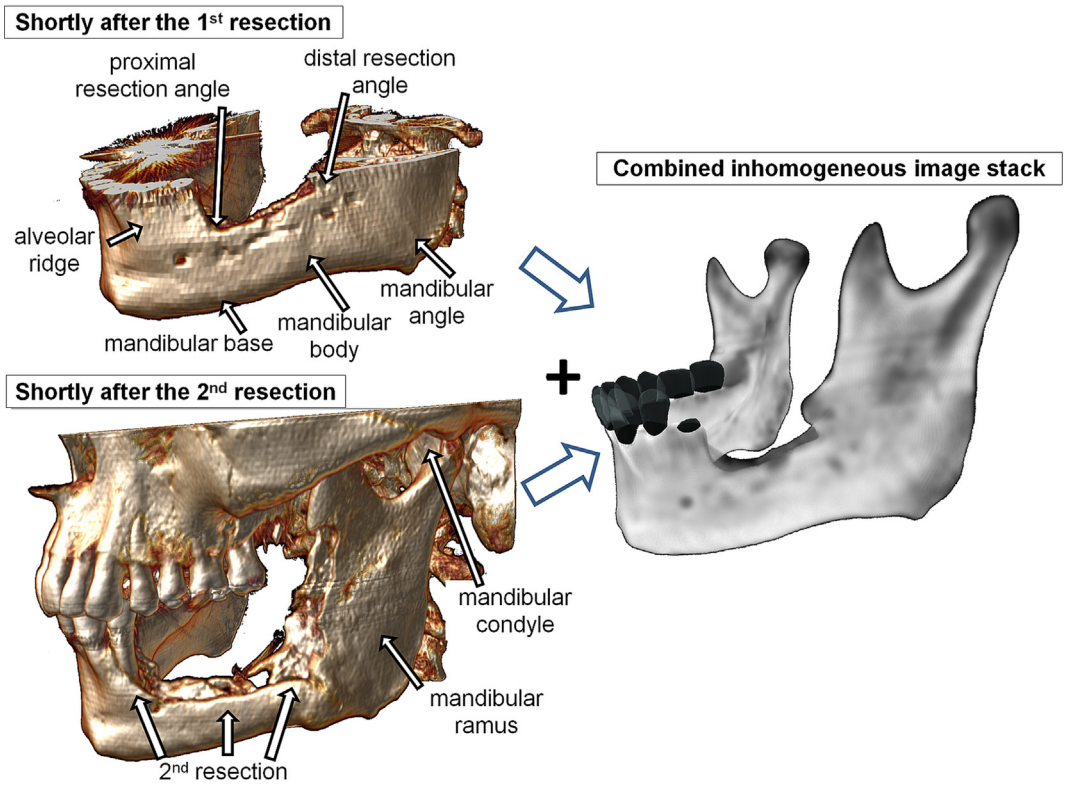

Fig. 1. Left: mandibular anatomy shortly after first and second resection, based on CT-follow-up 3 (top) and CT-follow-up 6 (bottom), displayed by shaded volume rendering, right: 3D-visualization of the combined mandibular image data by transparent volume rendering.

Table 1
Acquisition parameters of the follow-up-CT's before hemimandibulectomy (CT: LightSpeed QX/i, GE Medical Systems).

	Date of acquisition	kvp	X-ray tube current	Axial pixel side length	Slice thickness	Imaged part of the mandible
1	10/2009	120 V	60 mA	0.3125 mm	1.25 mm	Mandibular body (plus partially the mandibular rami for follow-up-CT 5)
2	03/2011			0.2617 mm		
3	08/2011, after 1st resection					
4	11/2011					
5	05/2012					
6	10/2013, after 2nd resection		80 mA	0.3711 mm	0.4 mm	Complete mandible

joint (TMJ) capsules, discs, and ligaments were segmented. The segmented TMJ tissues were combined and modified to simplified TMJ capsules (Fig. 2c) allowing, as part of the simulation model, small condylar displacements (Kober et al., 2015). Owing to Saint-Venant's principle (von Mises, 1945), enough far from the loaded tooth, the load absorbing effect of the periodontal ligament (PDL) can be approximated by reduced biting forces. Therefore, as in (Chou et al., 2015; Ertem et al., 2013; Pérez et al., 2010), the PDL was not modeled as separate tissue. Following (Erdmann et al., 2002), a tetrahedral FE-grid (682641 tetrahedrons, 131,091 nodes) was generated from this segmentation with adaptive refinement at the resection and the condyles (Fig. 2).

2.4. Inhomogeneous coefficients of skeletal elasticity

By adaptive refinement, ORN-related HU-values from CT could be mapped to the tetrahedrons of the FE-mesh in high resolution. Though a feasible procedure for mandibular anisotropic trajectories at hand (Kober et al., 2006), tissue anisotropy was neglected because of cortical disarrangement already visible in follow-up-CT 3 (Fig. 5c, red and black arrows). For model "M1-inhomog", we refer to the relations of HU-values to inhomogeneous, but isotropic elastic coefficients provided in (Hellmich et al., 2008). As derived for (not-radiated) human mandibular bone, these relations reflect the individual local micromechanical composition of bone, including resorption and osteosclerosis, but without the effect of radiation on the skeletal nanostructure. The latter is most likely negligible in the present context. For investigation of the influence of the skeletal compromise, two further models were analyzed, (i) "M2-strong" with standard "healthy" coefficients (Ertem et al., 2013) and (ii) "M3-mean" with coefficients averaged over cortical respectively trabecular elastic coefficients of M1-inhomog. The cortical Young's modulus of M3-mean is nearly half of M2-strong, probably due to ORN-related osteolysis, whereas the trabecular Young's modulus of M3-mean is nearly twice of M2-strong, suggesting osteosclerosis (Table 2).

2.5. Simulation concept

The model was rigidly constrained (Dirichlet boundary conditions) at the attachments of the TMJ-capsule to the skull (Fig. 2c). Neumann boundary conditions referring to non-zero

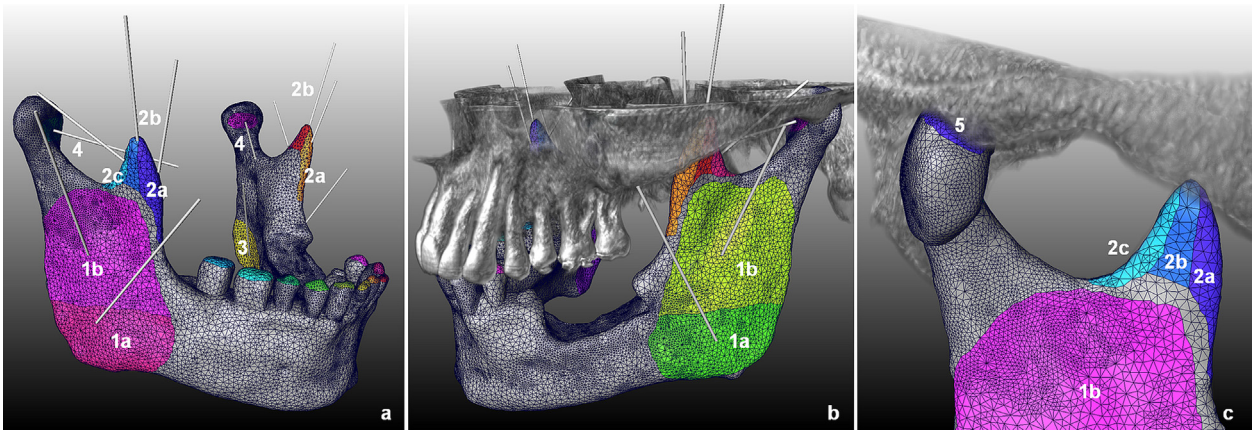

Fig. 2. Muscular attachments and directions, (a) contralateral, (b) ipsilateral, (c) mandibular condyle with TMJ capsule, 1: masseter muscle, 1a: superifical, 1b: deep portion, 2: temporal muscle, 2a: frontal, 2b: middle, 2c: posterior portion, 3: medial pterygoid muscle, 4: lateral pterygoid muscle, 5: attachment of the TMJ-capsule to the skull.

Table 2
Summary of applied elastic coefficients.

Model/tissue	Young's modulus E	Poisson's ratio ν	Reference
Model **M1-inhomog**	Inhomogeneous and isotropic relations for E and ν based on the HU-values of the combined data set		Hellmich et al., 2008
Model **M2-strong**:			
cortical bone	14.8 GPa	0.3	Ertem et al., 2013
trabecular bone	1.85 GPa	0.3	
Model **M3-mean**:			
cortical bone	7.69 GPa	0.314	
trabecular bone	3.40 GPa	0.344	
TMJ capsules	6.0 MPa	0.47	Korioth and Hannam, 1994
Teeth	17.6 GPa	0.25	

Table 3
Applied muscular forces, RMOL: contralateral first molar biting, INC: incisal biting, ICP: intercuspal position, LGF: lateral group effort.

	Forces [N] (Newton)					
Biting task	RMOL		INC	ICP	LGF	
Muscles	Right	Left	Right/left	Right/left	Right	Left
Superficial masseter	43.87	36.56	24.37	60.93	10.97	16.45
Deep masseter	18.8	15.67	6.79	26.11	9.4	6.79
Medial pterygoid	46.99	33.56	43.63	42.51	3.92	42.51
Frontal temporalis	36.91	29.32	4.04	49.55	33.37	3.54
Middle temporalis	20.19	20.50	1.84	29.37	19.58	1.84
Posterior temporalis	14.27	9.43	0.97	22.74	15.00	1.45
Lateral pterygoid	6.42	13.92	19.79	11.20	14.47	3.73
Anterior digastric	0.0	0.0	6.4	3.58	6.53	4.86

Table 4
Applied tooth forces, RMOL: contralateral first molar biting, INC: incisal biting, ICP: intercuspal position, LGF: lateral group effort.

	Forces [N] (Newton)										
	Right/contralateral						Ipsilateral/left				Sum
	2nd molar	1st molar	Premolar	Premolar	Canine	Incisor	Incisor	Incisor	Canine	Premolar	
RMOL	0	155.0	0	0	0	0	0	0	0	0	155.0
INC	0	0	0	0	0	11.4	7.6	11.4	0	0	30.4
ICP	88.0	44.0	18.5	6.0	18.5	0	0	0	18.5	6.0	199.5
LGF	10.5	2.5	8.0	9.0	13.0	0	0	0	0	0	43.0

forces were applied to muscular attachments and tooth crowns (Fig. 2, Tables 3 and 4). As moderate biting forces were considered (normally) producing physiological skeletal tissue reaction below the yield strain (Keaveny and Hayes, 1993; Biewener, 1993), the simulations refer to linear elasticity. The numerical background including error estimations has been described earlier (Erdmann et al., 2002).

2.6. Muscle and tooth forces

Masseter (superficial and deep compartment), temporal (frontal, middle, posterior portion), medial pterygoid, lateral pterygoid, and diagstric muscles were modeled by parallel force vectors distributed over their attachments (Fig. 2). For this purpose, individual information from follow-up-CT's was interpreted, underpinned by anatom-

ical knowledge (Baron and Debussy, 1979). Due to missing data, previous publications about mandibular FEA after marginal resection (Ertem et al., 2013; Murakami et al., 2011) referred to muscular forces measured for healthy subjects (e.g., Korioth and Hannam, 1994). However, clinical measurements (Curtis et al., 1997) reported severely reduced masticatory function after mandibular resection. Therefore, muscular forces of healthy subjects would seriously overestimate a resected mandible's routine loading. Furthermore, in pathological situations, the identification of muscle forces by e.g., minimization strategies (e.g., Curtis, 2011) seemed questionable. Therefore, an alternative approach was needed.

Following (Kober et al., 2015), we implemented kind of virtual mandibular test stand for model M1-inhomog with muscle and tooth forces as user input. We applied 155 N to the contralateral (right) first molar (RMOL). This force resulted from clinical measurements as maximal molar biting force among patients without mandibular reconstruction, slightly above the mean force (148 N ± 81 N) measured for patients with mandibular reconstruction (Curtis et al., 1997). We started using 20% of the (healthy) muscle forces provided in (Korioth and Hannam, 1994). The resulting mandibular displacement was displayed 200-times exaggerated. As long as the mandible was displaced downward, muscular forces were increased by steps of 1%, until the crown of the loaded tooth was lifted slightly above its original position indicating, that, now, the applied biting force could be compensated. Within this virtual experiment, the resected mandible needed 32% (31% was too small) of the muscle forces given in (Korioth and Hannam, 1994) to withstand 155 N (Table 3).

For clenching in intercuspal position (ICP), incisal biting (INC), and lateral group effort (LGF), we followed a vice-versa strategy applying 32% of the "healthy" muscle forces reported in (Korioth and Hannam, 1994). Starting with comparably high biting forces, these forces were decreased until the tooth edges were lifted slightly above their original position, mimicking successful biting. For INC, the pathological mandible is able to withstand forces of 11.4 N, 7.6 N, 11.4 N applied to its three residual incisors. This means that the patient is able to masticate food, which can be chewed by these forces, but cannot masticate food requiring higher forces. The summarized force 30.4 N lies within the range of incisal forces measured by (Curtis et al., 1997) for both, patients without mandibular reconstruction (43 N ± 18 N) and patients with mandibular reconstruction (69 N ± 41 N). Endorsed by this validation, we consider the results of the virtual biomechanical testing not as real, but realistic estimations of the patient's routine loading, notably individually adapted to this mandible's situation. All forces including for ICP and LGF are provided in Tables 3 and 4.

2.7. Evaluation of the simulation results

Maximal tensile and compressive volumetric strain is evaluated in seven anatomical regions: entire mandible R0, distal resection region R1, central resection region R2, proximal resection region R3, lower alveolar body below the resection R4, ipsilateral (left) condylar head and neck R5, contralateral (right) condylar head and neck R6, and contralateral mandibular half R7 (Fig. 4a). As the PDL was not respected as separate tissue, a region of about 1 mm around the loaded teeth was omitted from quantitative evaluation which was only relevant for compressive strain of R7 (ICP, RMOL) and R0 (RMOL).

For investigation of skeletal adaptation with unknown biting habits, other authors evaluated maximal values over a set of biting tasks (e.g., Curtis et al., 2011). In the present context, characteristic

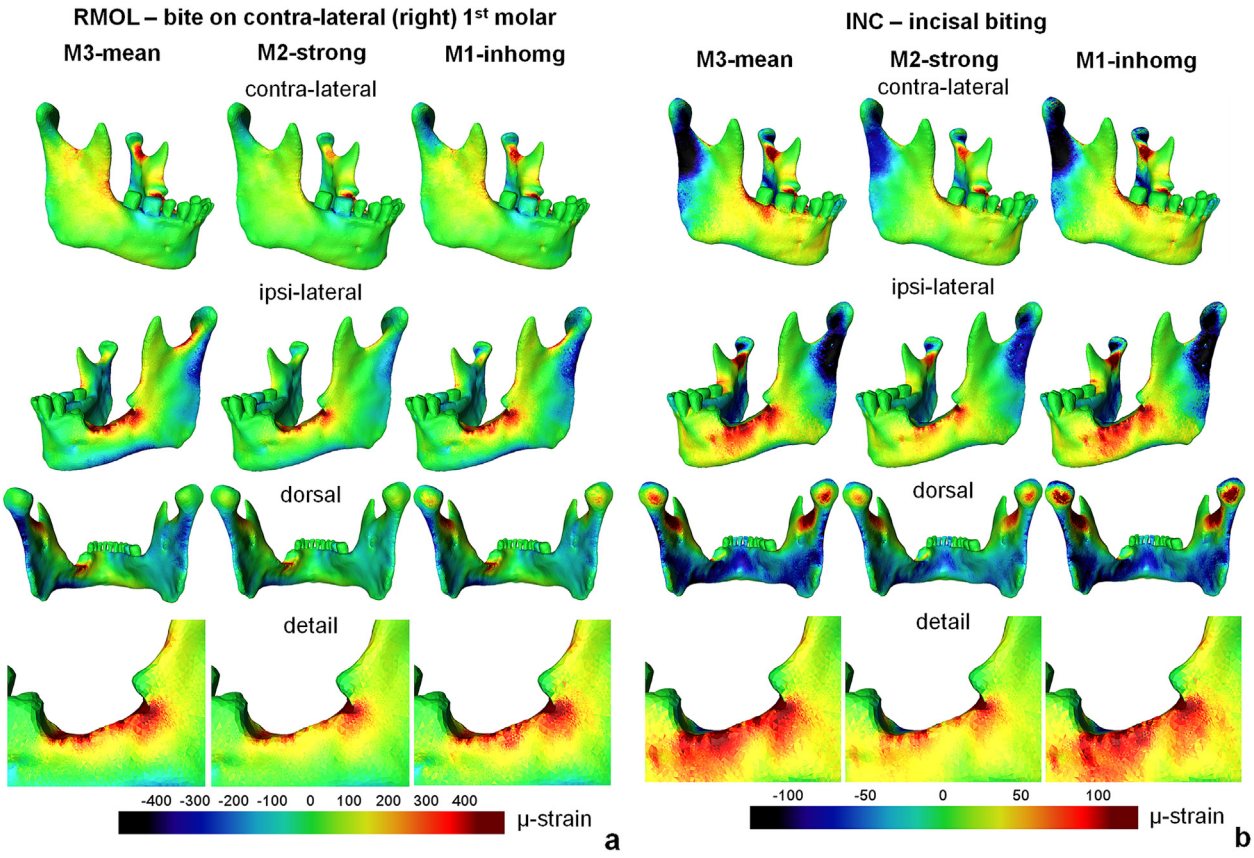

Fig. 3. Volumetric strain during (a) contralateral first molar biting (RMOL), (b) incisal biting (INC).

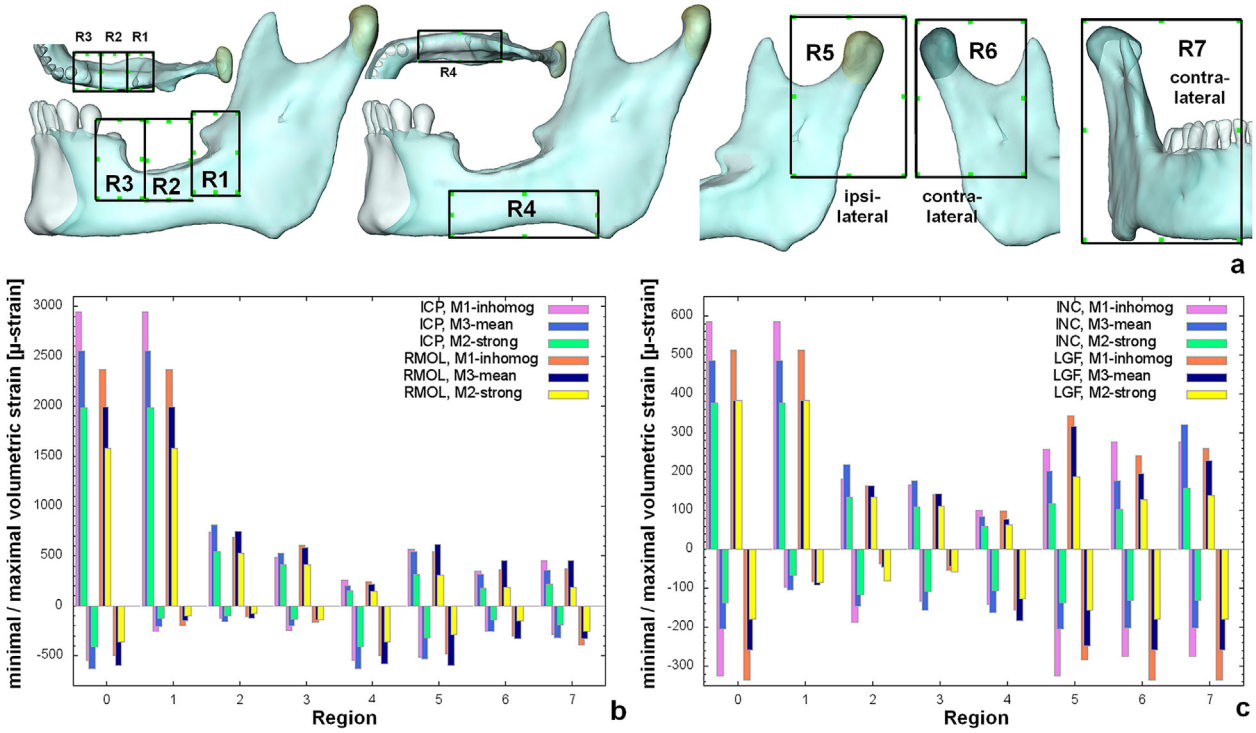

Fig. 4. (a) Anatomical regions for quantitative evaluation, R0: entire mandible, R1: distal resection region, R2: central resection region, R3: proximal resection region, R4: lower alveolar body below the resection, R5: ipsilateral (left) condylar head and neck, R6: contralateral (right) condylar head and neck, R7: contralateral mandibular half, (b and c) maximal tensile (positive values) and compressive (negative values) volumetric strain in R0–R7, muscle and bite forces given in Tables 3 and 4.

features of the strain distribution over the ipsilateral alveolar body are comparable for all tested biting tasks (Figs. 3 and 4). Clinically, patients with unilateral pathology tend to contralateral biting. Therefore, we chose contralateral first molar biting RMOL (Fig. 5d) for immediate comparison with the visualization of the skeletal tissue, keeping in mind the possible influence of other biting tasks.

3. Results

3.1. Evaluation of volumetric strain

For all load cases, dominant tensile strain is observed in the distal resection region R1, caused by the sharp resection angle (Figs. 3 and 4b,c). Though moderate biting forces, the strain of M1-inhomog for biting task ICP is near 3000 µstrain (Fig. 4b) reported as critical value for skeletal damage (Frost, 1987; Frost, 2003; Murakami et al., 2011). Due to the reduced alveolar height and the proximal resection corner, elevated tensile strain occurred in the central (R2) and proximal (R3) resection regions, but reduced by 68–75% compared to R1. Region R4 below the resection shows elevated compressive strain at similar level. By higher biting forces, volumetric strain during ICP and RMOL exceeded the load during INC and LGF. Though contralateral focus of biting forces during ICP and RMOL, dominant strain turned ipsilaterally (Fig. 4b). Contrariwise, for INC and LGF with more anteriorly focused forces, mandibular rami and condyles (R5, R6) bore higher loads than R2-R4 (Fig. 4c). Generally, the resected side with the pathology (R1-R5) was subjected to considerably higher strain than the non-affected side (R6-R7).

The characteristic strain distribution with dominant peak in R1 and elevated strain in R2-R4 is similar for all models (Fig. 3). The "healthy" model M2-strong exhibited lower strain than the pathological models M1-inhomog and M3-mean, but with quantitative strain decrease less than 36% for R1 respectively 27% for R2 (Fig. 4b and c). Besides R1, M1-inhomog and M3-mean show similar strain.

3.2. Comparison of volumetric strain profiles and the development of the skeletal tissue

By transparent 3D-visualization (Kober and Kjeller, 2015), the development of the skeletal tissue is depicted over four years (Fig. 5a–c and e–g). The visualization is linked to HU-values from CT, so red color refers to high bone mineralization, whereas dark blue color stands for low bone mineralization showing possible destructive alterations. Due to the limited FoV of the follow-up-CT's (Table 1), this analysis is restricted to the (ipsilateral) alveolar body.

From 10/2009, ongoing lingual destruction is observed, progressing from distal to proximal (Fig. 5a and b, left images, black arrows). In the visualization at 08/2011, it is apparent that the lingual proximal resection margin is well adapted to these destructions (Fig. 5c, left image, black arrow). In the lingual volumetric strain profile, slightly elevated tensile strain is there observed, caused by anatomical changes and weakened skeletal structure (Fig. 5d, left image, black arrow). In the sequel, we there find ongoing cortical destruction, progressing proximally from tooth to tooth (Fig. 5e–g, left column, black arrows).

Comparably moderate buccal resorption was observed before 08/2011 (Fig. 5a and b, right images, dotted black arrows). In the visualization at 03/2011, a small lesion near the mental foramen appeared, expanded towards the proximal resection angle in 08/2011 (Fig. 5b and c, right images, black arrows). The simulation shows elevated tensile strain (Fig. 5d, right image, black arrow). Still moderate in 11/2011, skeletal destruction there is progressing from 05/2012 and onwards (Fig. 5e–g, right images, black arrows). Likewise, the biting tasks INC and LGF show elevated tensile strain in the proximal resection angle (Fig. 3b).

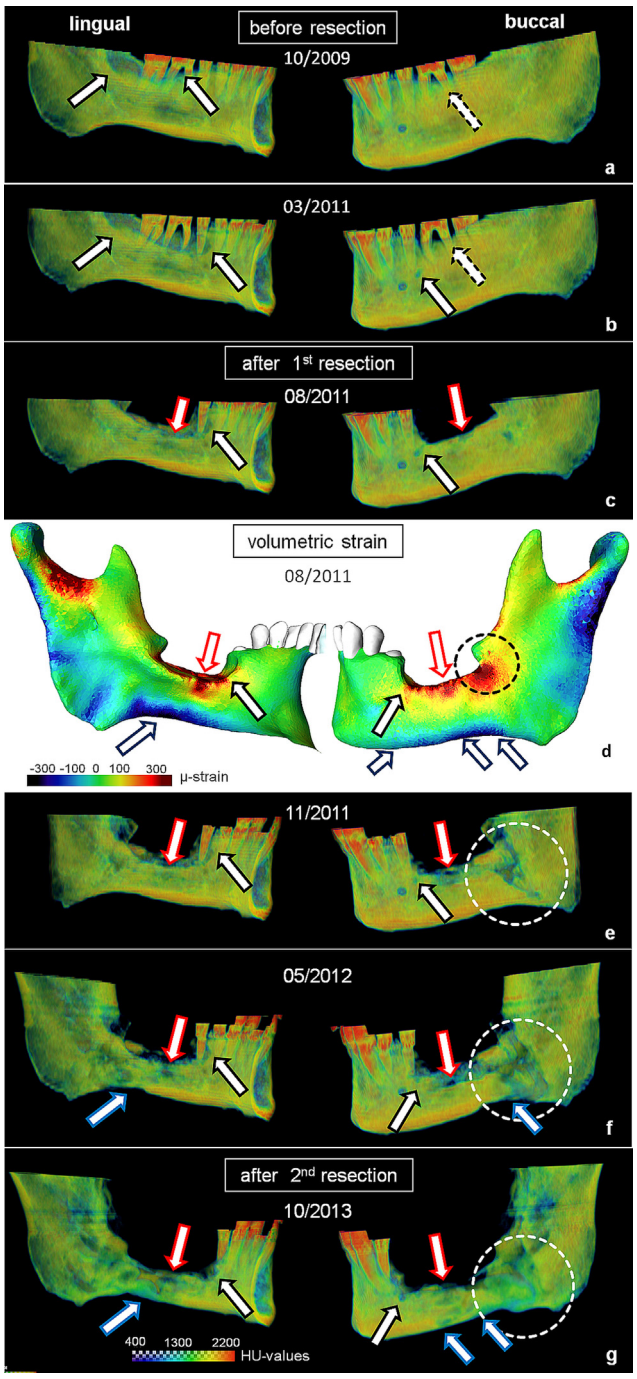

Fig. 5. (a–c) Visualization of the skeletal structure until the first resection, (d) ipsilateral volumetric strain during contralateral first molar biting (RMOL) referring to the situation after the first resection, (e–g) visualization of the skeletal structure, starting three months after the first resection.

In the visualization at 08/2011, local lingual and buccal lesions at the resection surface are seen, presumably ORN-related and present already before resection (Fig. 5c, red arrows). Most likely entailed thereby, the simulation there shows a band of locally elevated tensile strain from lingual to buccal (Fig. 5d, red arrows). At the lingual side, we can follow this (local) lesion from 11/2011 to 10/2013 (Fig. 5e–g, left images, red arrows). However, at the buccal side, we find continuous widening and lowering of the entire resection margin corresponding to elevated tensile strain there (Fig. 5d–g, right images, red arrows). From a biomechanical view, the local strain peaks were caused by ORN-related tissue compromise, whereas the elevated strain over the entire buccal resection margin was due to reduced alveolar height and missing teeth.

For all biting tasks, very high tensile strain occurred in the buccal distal resection corner (Figs. 3 and 5d, right image, circle). Biomechanically, this peak is due to the sharp distal resection angle. From 11/2011, less than three months after the first resection, severe cortical destruction was stated there, severely worsening in the further course of the disease (Fig. 5e–g, right images, circles).

Compared to less pathological mandibular loading profiles (Kober et al., 2015), the mandibular base shows elevated compressive strain, starting near the mandibular angle and extended in proximal direction (Figs. 3 and 5d, blue arrows). The suggested biomechanical background is the missing resistance against the masticatory muscles' traction due to reduced alveolar height and missing teeth. Destructive lingual and buccal correspondences occurred from 05/2012 starting distally below the resection, proximally extended in 10/2013 (Fig. 5f and g, blue arrows).

In Table 5, the observations are outlined. Progressive lingual bone resorption already appeared before the first resection whereas severe buccal cortical destruction was observed after. The serious buccal destruction in the distal resection angle corresponding to dominant tensile strain appeared only three months after the first resection (Fig. 5d and e, circles, Fig. 4b, region R1). For comparison, the destructive changes at the (central and proximal) resection margin (regions R2–R3) and the mandibular base (region R4) developed to severe extent after 05/2012, namely more than five months later (Fig. 5d and f, blue and red arrows). The strain of R2–R4 is about one third of R1 (Fig. 4b, Table 5). Hence, in correspondence to higher unphysiological load, more serious and earlier skeletal alterations were found.

4. Discussion

By detailed FEA respecting – as far as possible and available – pathology-related anatomy, tissue quality, and biting capacity, severe qualitative and quantitative alterations of the physiological mandibular biomechanics were found as consequence of marginal mandibulectomy and progressive ORN. Simulations with healthy instead of pathological tissue coefficients showed qualitatively similar strain distribution with quantitative improvement less than 36%. Though very moderate biting forces, critical tensile strain peaks were observed in the distal resection corner followed by the central resection region. By 3D-visualizations of the progressing skeletal compromise over four years, remarkable correspondences of skeletal destruction and increased tensile or compressive volumetric strain were stated. Higher unphysiological load was correlated with more serious and earlier skeletal alterations.

The significance of volumetric strain for skeletal adaptation has been substantiated, e.g., in (Hellmich et al., 2008; Kober et al., 2006). Following poro-micro-mechanical analyses (Cowin, 1999; Hellmich and Ulm, 2005), predominantly the volumetric part of strains evokes fluid pressure changes in the skeletal nano- and microporosity. Based on the clear results and tests with von Mises equivalent strain, we expect comparable results for other indicator variables.

By Wolff's law (Wolff, 1892), the general requirements for skeletal adaptations due to pathological biomechanics are fulfilled. Numerous studies (e.g., Chou et al., 2015; Mahnama et al., 2013) endorsed the supposition of mandibular biomechanical adaptation at clinically relevant dimensions. Therefore, the observed correspondences of skeletal resorption and regionally increased strain raised the suggestion of decisive contribution of pathological biomechanics to the skeletal destruction for the considered case.

Table 5
Development of the skeletal inner structure and corresponding volumetric strain (model M1-inhomog, biting task RMOL, Fig. 4b), ordered according to their first observation, anatomical regions according to Fig. 4a.

	Alteration of skeletal inner structure (CT)	Corresponding maximal volumetric strain, anatomical region	Suggested background of elevated strain	First observed	Order of magnitude	Symbol in Fig. 5
	Observed before the first resection:					
1	Lingual destruction, starting distally, proximally progressing from tooth to tooth	Elevated tensile strain at the lingual proximal resection margin, R3, 611 μstrain	Entailed by ORN-related anatomical and skeletal changes	10/2009	First moderate, from 03/2011 remarkable	Black arrows
2	Buccal destruction, starting near the mental foramen, progressing to the proximal resection angle	Elevated tensile strain at the buccal proximal resection margin, R3, 611 μstrain	First entailed by ORN-related lesion, then also due to the proximal resection angle	03/2011	First small, from 05/2012 remarkable	Black arrows
	Observed post-operatively, in the CT at 08/2011:					
3	Local ORN-related lesions near the middle of resection surface, lingual and buccal	Band of elevated tensile strain from buccal to lingual, R2, 690 μstrain	Entailed by local ORN-related skeletal lesion	08/2011	Local, but deepened from 05/2012	Red arrows
	Observed after the first resection:					
4	Widened and lowered buccal resection margin	Elevated tensile strain over the (entire) buccal resection margin, R2, R3, 690 μstrain	Reduced alveolar height, missing teeth	11/2011	First moderate, from 05/2012 remarkable	Red arrows
5	Massive buccal destruction at the distal resection angle	Very high tensile strain peak, R1, 2366 μstrain	Sharp distal resection angle	11/2011	To highest extent	Dotted black circles
6	Destruction at the mandibular base, starting distally, progressing in proximal direction	High compressive strain at mandibular base, extended in proximal direction, R4, −499 μstrain	Reduced alveolar height, missing teeth	05/2012	Medium in this context	Blue arrows

The question arises how far these results are generally relevant for patients after mandibular box resection, e.g., oral cancer patients without osteonecrosis. Mechanical stress concentrations in sharp angles are fundamental engineering knowledge (e.g., Savruk and Kazburek, 2016; Yosibash, 2011). Therefore, the peak load in the distal resection angle is a universal phenomenon confirmed by previous numerical and experimental studies (e.g., Ertem et al., 2013; Murakami et al., 2011). The same applies to mechanical alterations due to reduced alveolar height, albeit to lower degree (e.g., Murakami et al., 2011). In the present study, simulations with healthy tissue coefficients showed unphysiological strain distributions independently from skeletal pathologies (Fig. 3). This implies the immanent danger of highly pathological biomechanics and – following Wolff's law – severe skeletal adaptations generally for patients after mandibular box resection.

For patients with skeletal pathologies undergoing mandibular box resection, there is the additional danger that small lesions of the bone entail elevated strain propagating through the tissue (e.g., Yosibash, 2011), see e.g., at the central and proximal resection margin for the considered case. As before, there is the risk of unwanted skeletal adaptations.

The presented results suggest that pathological biomechanics post resection, notably caused by own muscular activity, are a potential further burden for the affected patients besides primary diseases, e.g., oral cancer or osteonecrosis. Especially patients with good muscular and dental status are at risk. The considered patient was subjected to hemimandibulectomy about 2.5 years after the first resection. Due to very high efforts, this study was limited to one patient. Current research is dedicated to FEA of alternative resection patterns, e.g., arch-shaped rather than box-shaped. Most mandibular resections are serious interventions where any therapeutic regime, characterized by its assets and drawbacks, represents only a fragile trial to restore the situation before diagnosis. Taking biomechanical considerations into account potentially bears the chance to spare the patients from serious suffering.

Acknowledgements

This research was partially supported by the MIRACLE Project, University of Basel, funded by the Werner Siemens-Foundation, Switzerland. The authors acknowledge the Department of Oral and Maxillofacial Radiology at the Institute of Odontology, Sahlgrenska Academy, Gothenburg University, Sweden, for provision of the radiological data and Prof. H.-F. Zeilhofer, Basle, Switzerland for his continuous support of this research. The first author acknowledges H.-C. Hege, ZIB Berlin, and R. Brandt, Thermo Fisher Scientific, both Berlin, Germany, for the Amira® license, as well as K. and W. Habersack, Munich, Germany, for advice from orthodontics. Finally, all authors sincerely thank Professor em. J. M. Hirsch, Stockholm, Sweden, for initiating this research.

Sources of funding

This study was partially supported by the MIRACLE Project, University of Basel, which is funded by the Werner Siemens-Foundation, Switzerland. The first author Cornelia Kober received a free license of the Amira® software by the Zuse Institute Berlin (ZIB), and the Company Thermo Fisher Scientific, both Berlin, Germany.

Declaration of Competing Interest

All authors declare that they have no conflict of interest. The authors had no writing assistance. There was no influence on the study design, the collection, analysis, or interpretation of the data, the writing of the manuscript, or the decision to submit the manuscript for publication.

Ethical approvals

All procedures performed in studies involving human participants were in accordance with the ethical standards of the institutional and/or national research committee and with the 1964 Helsinki declaration, its later amendments, or comparable ethical standards. For this retrospective analysis, formal consent is not required. Informed consent is also not required. This article does not contain any studies with animals performed by any of the authors.

Appendix A. Supplementary material

Supplementary data to this article can be found online at https://doi.org/10.1016/j.jbiomech.2019.109320.

References

Baron, P., Debussy, T., 1979. A biomechanical functional analysis of the masticatory muscles in man. Arch. Oral Biol. 24 (7), 547–553.

Biewener, A.A., 1993. Safety factors in bone strength. Calcif. Tissue Int. 53 (Suppl 1), 68–74.

Chou, H.Y., Jagodnik, J.J., Müftü, S., 2008. Predictions of bone remodeling around dental implant systems. J. Biomech. 41 (6), 1365–1373.

Chou, H.Y., Satpute, D., Müftü, A., Mukundan, S., Müftü, S., 2015. Influence of mastication and edentulism on mandibular bone density. Comput. Method. Biomech. Biomed. Eng. 18 (3), 269–281.

Cowin, S.C., 1999. Bone poroelasticity. J. Biomech. 32, 217–238.

Curtis, D.A., Plesh, O., Miller, A.J., Curtis, T.A., Sharma, A., Schweitzer, R., Hilsinger, R. L., Schour, L., Singer, M., 1997. A comparison of masticatory function in patients with or without reconstruction of the mandible. Head Neck 19 (4), 287–296.

Curtis, N., Jones, M.E.H., Shi, J., O'Higgins, P., Evans, S.E., Fagan, M.J., 2011. Functional relationship between skull form and feeding mechanics in Sphenodon, and implications for diapsid skull development. PLoS ONE 6 (12), e29804.

Daegling, D.J., Hylander, W.L., 2000. Experimental observation, theoretical models, and biomechanical inference in the study of mandibular form. Am. J. Phys. Anthropol. 112 (4), 541–551.

Erdmann, B., Lang, J., Roitzsch, R., 1993. Kaskade Manual – version 2.0. Technical report TR-93-05, ZIB Berlin, Berlin. urn:nbn:de:0297-zib-4970. (https://opus4.kobv.de/opus4-zib/frontdoor/index/index/docId/497).

Erdmann, B., Kober, C., Lang, J., Deuflhard, P., Zeilhofer, H.-F., Sader, R., 2002. Efficient and reliable finite element methods for simulation of the human mandible. In: The finite element method in biomedical engineering, biomechanics and related fields [CD-ROM] University of Ulm, Ulm. see also ZIB Report ZR-01-14. ZIB Berlin. Berlin. urn:nbn:de:0297-zib-6403. (https://opus4.kobv.de/opus4-zib/frontdoor/index/index/docId/640).

Ertem, S.Y., Uckan, S., Ozden, U.A., 2013. The comparison of angular and curvilinear marginal mandibulectomy on force distribution with three dimensional finite element analysis. J. Craniomaxillofac. Surg. 41, e54–e58.

Frost, H.M., 1987. Bone "mass" and the "mechanostat": a proposal. Anato. Rec. 219 (1), 1–9.

Frost, H.M., 1994. Wolff's Law and bone's structural adaptations to mechanical usage: an overview for clinicians. Angle Orthodont. 64 (3), 175–188.

Frost, H.M., 2003. Bone's Mechanostat: A 2003 Update The anatomical record. Part A. Dis. Mol., Cell. Evol. Biol. 275 (2), 1081–1101.

Gröning, F., Fagan, M., O'Higgins, P., 2012. Comparing the distribution of strains with the distribution of bone tissue in a human mandible: a finite element study. Anatom. Rec. 296, 9–18.

Hellmich, C., Kober, C., Erdmann, B., 2008. Micromechanics-based conversion of CT data into anisotropic elasticity tensors, applied to FE simulations of a mandible. Ann. Biomed. Eng. 36 (1), 108–122.

Hellmich, C., Ulm, F.-J., 2005. Drained and undrained poroelastic properties of healthy and pathological bone: a poro-micromechanical investigation. Transp. Porous Media 58, 243–268.

Kalender, W.A., 2011. Computed Tomography: Fundamentals, System Technology, Image Quality, Applications. Wiley, Weinheim.

Keaveny, T.M., Hayes, W.C., 1993. Mechanical Properties of Cortical and Trabecular Bone. CRC Press, Boca Raton, pp. 285–344.

Kober, C., Erdmann, B., Sader, R., Zeilhofer, H.-F., 2003. Simulation of the human mandible: comparison of bone mineral density and stress/strain profiles due to masticatory muscles' traction. In: The finite element method in biomedical engineering, biomechanics and related fields [CD-ROM] University of Ulm, Ulm. see also ZIB-Report ZR-03-23. ZIB Berlin. urn:nbn:de:0297-zib-7458 (https://opus4.kobv.de/opus4-zib/frontdoor/index/index/docId/745).

Kober, C., Erdmann, B., Hellmich, C., Sader, R., Zeilhofer, H.-F., 2006. Consideration of anisotropic elasticity minimizes volumetric rather than shear deformation in human mandible. Comput. Methods Biomech. Biomed. Eng. 9 (2), 91–101.

Kober, C., Hellmich, C., Stübinger, S., Zeilhofer, H.-F., Sader, R., 2015. "Anatomical simulation" of the biomechanical behavior of the human mandible. Int. J. Comput. Dent. 18 (4), 333–342.

Kober, C., Kjeller, G., 2015. A Computer assisted method for assessment of mandibular osteoradionecrosis for local screening and detection of periled region. Int. J. Comput. Assist. Radiol. Surg. 10 (Suppl 1), S145–S146.

Kober, C., Berg, B.-I., Hellmich, C., Sader, R., Kjeller, G., 2016. Mandibular finite element analysis after partial alveolar ridge resection due to progressive osteoradionecrosis. Int. J. Comput. Assist. Radiol. Surg. 11 (Suppl 1), S142–S143.

Kober, C., Hellmich, C., Gurin, A., Komlev, V.S., Kjeller, G., Sader, R., Zeilhofer, H.-F., Berg, B.-I., 2017. Pathological mandibular biomechanics: finite element analysis based on partial dentition, cystic lesion, and partial resection. Int. J. Comput. Assist. Radiol. Surg. 12 (Suppl 1), S170–S172.

Korioth, T.W., Hannam, A.G., 1994. Mandibular forces during simulated tooth clenching. J. Orofac. Pain 8 (2), 178–189.

Li, K., Xin, H., Zhao, Y., Zhang, Z., Wu, Y., 2016. Remodeling of the mandibular bone induced by overdentures supported by different numbers of implants. J. Biomech. Eng. 138 (5), 051003. https://doi.org/10.1115/1.4032937.

Mahnama, A., Tafazzoli-Shadpour, M., Geramipanah, F., Mehdi Dehghan, M., 2013. Verification of the mechanostat theory in mandible remodeling after tooth extraction: animal study and numerical modeling. J. Mech. Behav. Biomed. Mater. 20, 354–362.

Massa, S.T., Cass, L.M., Osazuwa-Peters, N., Christopher, K.M., Walker, R.J., Varvares, M.A., 2017. Decreased cancer-independent life expectancy in the head and neck cancer population. Head Neck 39, 1845–1853.

Muñoz Guerra, M.F., Naval Gías, L., Campo, F.R., Pérez, J.S., 2003. Marginal and segmental mandibulectomy in patients with oral cancer: a statistical analysis of 106 cases. J. Oral Maxillofac. Surg. 61 (11), 1289–1296.

Murakami, K., Sugiura, T., Yamamoto, K., Kawakami, M., Kang, Y.B., Tsutsumi, S., Kirita, T., 2011. Biomechanical analysis of the strength of the mandible after marginal resection. J. Oral Maxillofac. Surg. 69 (6), 1798–1806.

Obinata, K., Shirai, S., Ito, I., Nakamura, M., Carrozzo, M., Macleod, I., Carr, A., Yamazaki, Y., Tei, K., 2017. Image findings of bisphosphonate related osteonecrosis of jaws comparing with osteoradionecrosis. Dentomaxillofac. Radiol. 46, 20160281.

Pérez, M.A., Fornells, P., Doblaré, M., García-Aznar, J.M., 2010. Comparative analysis of bone remodelling models with respect to computerised tomography-based finite element models of bone. Comput. Methods Biomech. Biomed. Eng. 13 (1), 71–80.

Reina, J.M., García-Aznar, J.M., Domínguez, J., Doblaré, M., 2007. Numerical estimation of bone density and elastic constants distribution in a human mandible. J. Biomech. 40 (4), 828–836.

Savruk, M.P., Kazburek, A., 2016. Stress Concentration at Notches. Springer, Cham.

Stalling, D., Westerhoff, M., Hege, H.C., 2005. Amira: A Highly Interactive System for Visual Data Analysis. In: Hansen, C.D., Johnson, C.R. (Eds.), The Visualization Handbook. Elsevier, Amsterdam, pp. 749–767.

Suenaga, H., Chen, J., Yamaguchi, K., Li, W., Sasaki, K., Swain, M., Li, Q., 2015. Mechanobiological bone reaction quantified by positron emission tomography. J. Dent. Res. 94 (5), 738–744.

Vijayaraghavan, N.V., Ramesh, G., Thareja, A., Patil, S., 2015. Masticatory efficiency after rehabilitation of acquired maxillary and mandibular defects. Ind. J. Dent. 6 (3), 139–146.

von Mises, R., 1945. On Saint-Venant's Principle. Bull. Am. Math. Soc. 51, 555–562.

Wang, C., Han, J., Li, Q., Wang, L., Fan, Y., 2014. Simulation of bone remodelling in orthodontic treatment. Comput. Methods Biomech. Biomed. Eng. 17 (9), 1042–1050.

Wax, M.K., 2005. Preservation of the mandible in the management of cancer of the oral cavity. Operat. Tech. Otolaryn.-Head Neck Surg. 16 (1), 18–23.

Williams, S.H., Vinyard, C.J., Wall, C.E., Hylander, W.L., 2009. Mandibular corpus bone strain in goats and alpacas: implications for understanding the biomechanics of mandibular form in selenodont artiodactyls. J. Anat. 214, 65–78.

Wolff, J., 1892. Das Gesetz der Transformation der Knochen. Hirschwald, Berlin.

Yosibash, Z., 2011. Singularities in Elliptic Boundary Value Problems and Elasticity and Their Connection with Failure Initiation. Springer Science & Business Media, New York.